

## Changes in marine hot and cold extremes in the China Seas during 1982–2020



Yan Li <sup>a,\*</sup>, Guoyu Ren <sup>b,c</sup>, Qingyuan Wang <sup>d</sup>, Lin Mu <sup>a</sup>

<sup>a</sup> College of Life Sciences and Oceanography, Shenzhen University, Shenzhen, China

<sup>b</sup> Department of Atmospheric Science, School of Environmental Studies, China University of Geosciences, Wuhan, China

<sup>c</sup> Laboratory for Climate Studies, National Climate Center, China Meteorological Administration, Beijing, China

<sup>d</sup> Tianjin Meteorological Observatory, China Meteorological Administration, Tianjin, China

### ARTICLE INFO

#### Keywords:

Marine heatwave  
Marine cold-spell  
Sea surface temperature  
China Seas

### ABSTRACT

Extremes in sea surface temperature (SST) have the potential to threaten marine biodiversity, ecosystem functions, and regional services. Using the OISST v2 data, we analyzed the spatial and temporal variability of marine hot and cold events in the China Seas during 1982–2020. Results showed that in majority of the China Seas, frequency of Hot Days (HDs) and Marine heatwaves (MHWs) has significantly increased; severe MHWs (SMHWs) have become more intense. Frequency of Cold Days (CDs) and Marine cold-spells (MCSs) has fallen dramatically; severe MCSs (SMCSs) have become weaker. All of the trend distributions are heterogeneous, with the largest magnitudes along the coast. Long-term temporal analysis revealed that cold extremes (CDs, MCSs, SMCSs) decreased significantly, while hot extremes (HDs, MHWs, SMHWs) increased at a higher confidence level and at a faster rate. Asymmetry characterizes the tendencies of hot and cold extremes. Further study demonstrated that mean SST warming, not SST variability, was the primary driver of trends in both MHW and MCS metrics. MHWs/MCSs related to the anthropogenic or natural forcing increased very rapidly in the post-1998 era.

### 1. Introduction

The most recent Intergovernmental Panel on Climate Change (IPCC) report showed that it was an “established fact” that human-caused greenhouse gases (GHGs) emissions have already caused many changes in weather and climate extremes globally. According to extensive scientific research, terrestrial hot extremes (e.g. heatwaves) have become more frequent and intense across most land regions since the 1950s, while cold extremes (e.g. cold-spells) have become less frequent and severe (Zhang et al., 2019; Wang et al., 2022). However, in comparison to terrestrial extremes, marine extremes had remained largely unknown for a long time. Marine heatwaves (MHWs), refer to abnormally high temperature in the ocean that last at least 5 consecutive hot days (HDs) (Hobday et al., 2016, 2018). Their dramatic negative impacts on marine species, habitats, and even fisheries and aquaculture have been widely reported and confirmed (Hughes et al., 2017; Arias-Ortiz et al., 2018; Smale et al., 2019). Recently, there has been increasing attention on MHWs due to global warming (Laufkötter et al., 2020; Oliver et al., 2021). In contrast, their cool counterparts, marine cold-spells (MCSs) — periods of extremely cold water, still receive less

attention, despite the fact that MCSs also have the potential to harm marine ecosystem and commercial fisheries (Matich et al., 2020; Schlegel et al., 2021). Studies have been conducted to examine the characteristics and ecological impacts of marine extremes at the global and ocean basin scales (Darmaraki et al., 2019; Wang et al., 2022), but with significant gaps in the China Seas. Especially, researches on spatial-temporal characteristics and long-term trends of MCSs are still deficient.

The China Seas, which are part of the western Pacific Ocean and have an approximate range of (15°–45°N, 105°–130°E), are located on the southeastern edge of the Eurasian continent (Fig. 1). They consist of four marginal seas, known as the Bohai Sea, Yellow Sea, East China Sea, and South China Sea. The Kuroshio Current is a powerful western boundary current in this area which transports warm equatorial water as well as nutrients and sediment to mid to high latitude seas (Fig. 1, red line). There are numerous marine biological communities and commercial fisheries areas in coastal China that are critical to the sustainable development of society and economy. It is necessary to examine the behaviors of marine extremes in this region and assess the roles of externally forcing on the occurrence of the extremes.

\* Corresponding author.

E-mail address: [liyan\\_ocean@szu.edu.cn](mailto:liyan_ocean@szu.edu.cn) (Y. Li).

Using a high-resolution satellite product, we conduct a detailed investigation of the spatiotemporal variability of marine temperature extremes over the past four decades. Oliver (2019) demonstrated that a shift in the mean state, rather than changes in SST variability, can explain much of the increase in MHWs frequency in most part of the global ocean, but there is a need to examine the contributions at regional scale. Thus, we further look into whether and how much external forcing has contributed to the changing likelihood of MHWs and MCSs.

## 2. Dataset and methods

### 2.1. Sea surface temperature (SST) data

The  $0.25^\circ \times 0.25^\circ$  Daily SST data came from NOAA OISST v2.1, which covers the period from 1 Jan 1982 to 31 Dec 2020 (Banzon et al., 2016, 2020) (available online: [www.esrl.noaa.gov/psd/data/gridded/data.noaa.oisst.v2.highres.html](http://www.esrl.noaa.gov/psd/data/gridded/data.noaa.oisst.v2.highres.html)). OISST v2.1 incorporated Advanced Very High-Resolution Radiometer (AVHRR) infrared satellite SST from the Pathfinder satellite, in situ observations, buoy, ship. As the first available and longest time series of satellite-derived SST product, it is increasingly and widely used in research for SST extremes (Lima and Wethey, 2012; Benthuysen et al., 2018).

### 2.2. Defining SST extremes

Following in the footsteps of previous research, we focused on marine hot and cold extremes. Six metrics were used to describe the frequency and intensity properties of these extremes (Table 1). In case of temperature-based metrics, the number of HD/Cold Day (hereafter, 'CD') in each year was defined as the days when daily SST exceeding the 90th percentile/below 10th percentile of the baseline period of 1983–2012 in each year. The number of days exceeding or below such threshold is the simplest way to reveal the change of frequency behavior and interpret the shift of the distribution in SST. As to this calculation method, HD and CD mainly occurred in boreal summertime with a higher absolute value and in boreal wintertime with a lower absolute value, respectively. In our work, we adopted a qualitative definition proposed by Hobday et al. (2016) and Schlegel et al. (2017). According to their definitions, MHW/MCS was identified as local SST anomalies (SSTAs) exceeding/below the 90th/10th percentile threshold for at least 5 consecutive days, due to seawater's higher heat storage capacity than the atmosphere (3 days for the atmosphere heatwave). Here, relative thresholds were chosen to be high/low since MHW/MCS are considered extreme events, i.e. tails of anomalies distribution. The 90th/10th percentile thresholds were calculated from data within an 11-day

**Table 1**

List of selected metrics based on relative thresholds measuring the marine temperature extremes characteristics.

Metrics	ID	Definition
Hot Day	HD	The day when daily SST > 90th percentile threshold of 1983–2012 baseline period
Cold Day	CD	The day when daily SST < 10th percentile threshold of 1983–2012 baseline period
Marine heatwave	MHW	Warm and discrete event with high SSTA prolonged for more than 5 consecutive days
Marine cold-spell	MCS	Cold and discrete event with low SSTA prolonged for more than 5 consecutive days
Severe MHW	SMHWI	The largest intensity among all MHWs in each year
	SMHWD	The longest duration among all MHWs in each year
Severe MCS	SMCSI	The largest intensity among all MCSs in each year
	SMCSD	The longest duration among all MCSs in each year

window centered on each calendar day across 1983–2012 and then smoothed by a 31-day moving average. Two consecutive MHWs/MCSs with an interval of less than 2 days below the thresholds were considered as a single event. Using this 'day-specific' threshold allows for the detection and measurement of MHWs/MCSs at any times of the year. Severe MHWs/MCSs, characterized by their long duration and/or high intensity, would cause unacceptably multiple fatalities and/or overwhelming fishing economic losses. Severe MHWs/MCSs are defined as the largest intensity and longest duration among all MHWs/MCSs in each year. Duration was calculated as a time interval between the start time and end time of each MHW/MCS. Intensity was quantified by the highest/lowest SSTA in each single event (Hobday et al., 2016). Because MCS intensities are negative values, positive (negative) trends (seen Fig. 3f) indicate a weakening (strengthening) MCS.

Our work was conducted on both a regional basis and a per-grid basis. Regional average is calculated by area-weighted averaging the grid data using latitude cosine as weights. The nonparametric Mann-Kendall (MK) test was applied to determine the significance of the monotonic trend in temperature extreme indices. Similarly, the nonparametric estimator test (Sen, 1968) was employed to quantify the slope of the trend in temperature extreme indices.

### 2.3. Probability density functions (PDFs) and generalized extreme value (GEV)-fit

In probability theory and statistics, a PDF, or density of a continuous random variable, is a function that describes the relative likelihood for this random variable to take on a given value. Here, PDFs are calculated using the area-averaged daily SSTAs for the first decade 1982–1991 and

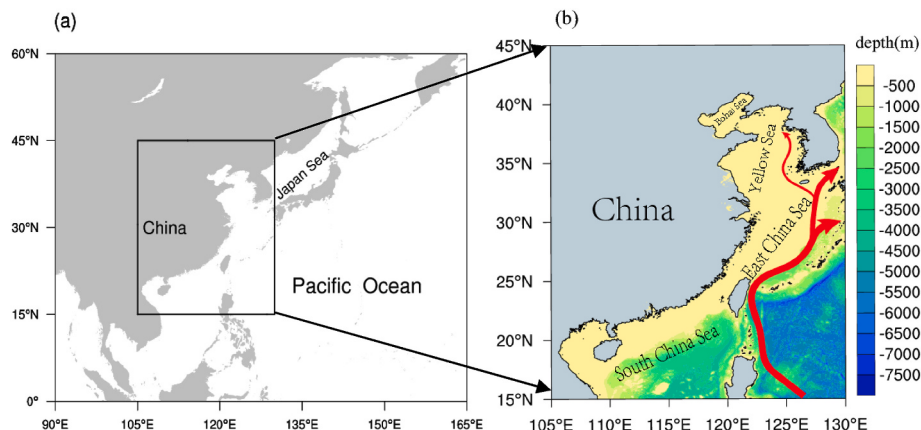


**Fig. 1.** Geographical maps of (a) the Northwest Pacific region, black rectangle indicates the China Seas and adjacent seas and (b) Map of the China Seas and adjacent seas with bathymetry (shaded areas, units: meters) (b), locations of the Bohai Sea, the Yellow Sea, the East China Sea (ECS) and the South China Sea (SCS) are depicted on the map. (For interpretation of the references to colour in this figure legend, the reader is referred to the Web version of this article.)

the last decade 2011–2020. Statistical characteristics of the PDFs, such as the higher moments (mean, variance and skewness), are also calculated. Before estimating the PDFs, the GEV-fit distribution is used. The GEV-fit distribution is a family of continuous probability distributions developed within extreme value theory to combine the Gumbel, Fréchet and Weibull families. The GEV distribution is widely employed in the environmental science to modelling extremes (Goubanova and Li 2007; Zwiers et al., 2011; Huang et al., 2016). Based on the extreme value theory that derives the GEV distribution, we fit a sample of extremes to the GEV distribution to obtain the parameters that best explains the probability distribution of very rare or extreme events.

#### 2.4. Mann-Kendall abrupt change test

The Mann-Kendall abrupt change test is one of the most effective methods for determining when an abrupt change occurred in a time series which has been used extensively in hydrological and meteorological climate change researches (Ullah et al., 2019a; Li et al., 2022). The abrupt change point is estimated by the series of progressive (*UF*) and retrograde (*UB*). If the *UF* and *UB* curves cross within the confidence zone, there will be a significant abrupt change point. Here, the 95% confidence level (1.96 and -1.96) was used as the confidence zone's borderlines (Tabari et al., 2012). The following are the calculating formulas:

For time series  $x_n$  ( $n$  is the length of the data set), the order series ( $S_k$ ) is given as follows:

$$S_k = \sum_{i=1}^k r_i, (k = 2, 3, 4, \dots, n)$$

In which,

$$r_i = \begin{cases} +1, & x_i > x_j, (j = 1, 2, 3, \dots, i) \\ 0, & x_i \leq x_j \end{cases}$$

Where  $x_i$  and  $x_j$  are the sequential data values, and the statistic (*UF* <sub>$k$</sub> ) is defined as:

$$UF_k = \frac{[S_k - E(S_k)]}{\sqrt{Var(S_k)}}, (k = 1, 2, 3, \dots, n)$$

Where  $UF_1 = 0$ ,  $E(S_k)$  and  $Var(S_k)$  are the average value and variance of  $S_k$ , which can be calculated by following equations:

$$E(S_k) = \frac{n(n+1)}{4}$$

$$Var(S_k) = \frac{n(n-1)(2n+5)}{72}$$

Then, the *UB* <sub>$k$</sub>  is calculated by repeating the above process in the order  $x_n, x_{n-1}, \dots, x_3, x_2, x_1$  of the time series which makes  $UB_k = UF_k (UB_1 = 0, k = n, n-1, \dots, 3, 2, 1)$ .

#### 2.5. Evaluation of roles of mean SST and its variability

To test whether trends of the MHW/MCS metrics are due to mean SST warming (i.e., positive shifts in the PDF, normally caused by anthropogenically forcing), internal variability (i.e., variance and skewness), or both, we follow the approach of Marin et al. (2020) and Chatterjee et al. (2022). Daily SST time series was decomposed into 'trend' daily SST ( $SST^{trend}$ ) and 'detrend' daily SST ( $SST^{detrend}$ ). MHW/MCS metrics from observed daily SST (referred to as  $MHW(SST)/MCS(SST)$ ) and 'detrended' daily SST (referred to as  $MHW(SST^{detrend})/MCS(SST^{detrend})$ ) are calculated respectively. MHWs metrics induced from mean SST warming, was identified by subtracting  $MHW(SST^{detrend})/MCS(SST^{detrend})$  from  $MHW(SST)/MCS(SST)$  (referred to as  $MHW(SST^{trend})/MCS(SST^{trend})$ ).

In accordance with Marin et al. (2020), the trend attributional ratio (TAR) of the mean SST and internal variability in long-term trends in MHW/MCS metrics was calculated as bellow.

$$TAR = \frac{|rate^{trend}| - |rate^{detrend}|}{\max(|rate^{trend}|, |rate^{detrend}|)} \quad (1)$$

where,  $|...|$  is the absolute value operator, and  $rate^{trend}$  and  $rate^{detrend}$  are MHW/MCS trends induced from mean SST warming and internal variability, respectively. Positive number implies that mean SST warming is the dominant driver of the trend; negative value suggests that internal variability is the primary driver.

### 3. Results

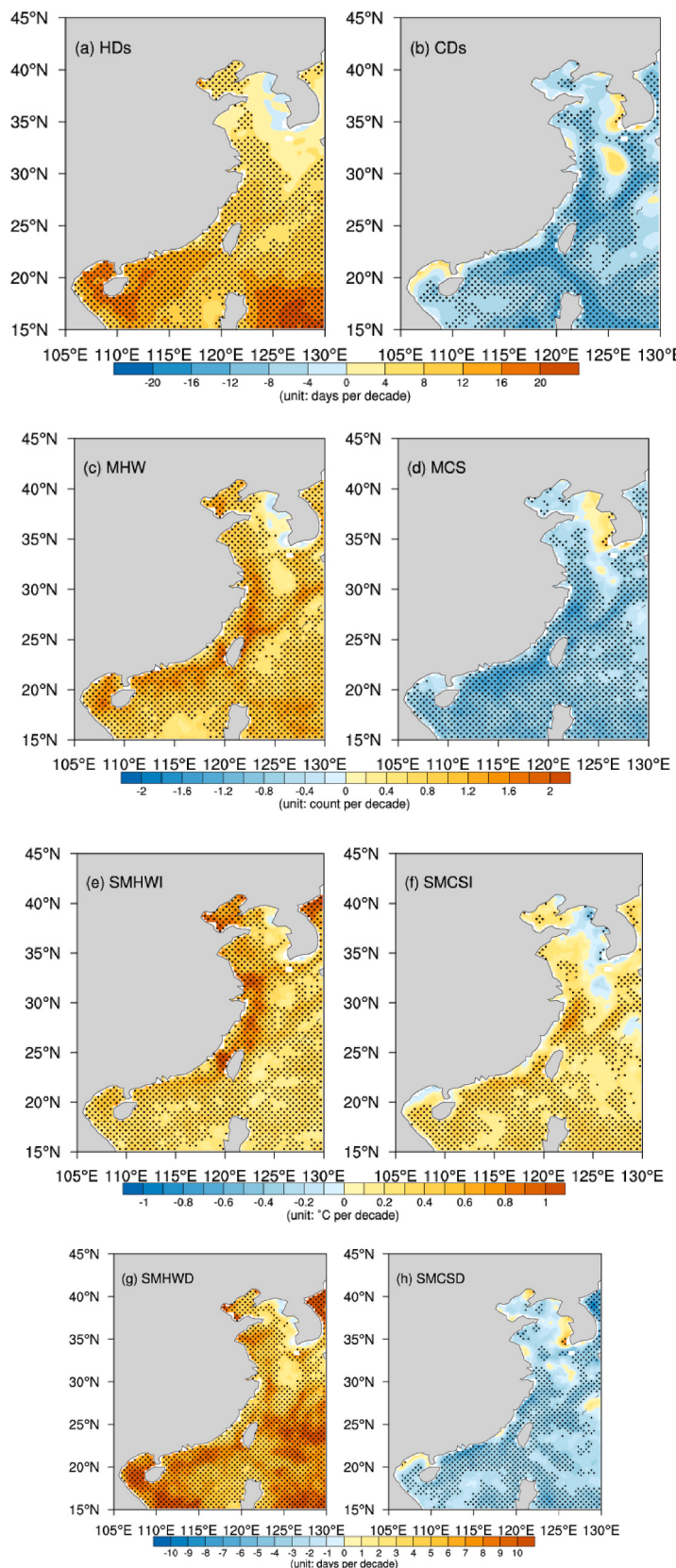
#### 3.1. Spatial variation of trends in marine temperature extremes

Fig. 2 depicts the regional distributions of the trends of marine hot and cold extremes in the China Seas from 1982 to 2020. With 95% confidence level, results revealed a regional rise in the hot extremes, including HDs, MHWs and strengthening of severe MHWs (Fig. 2a, b, 2c, 2d). Trends in HDs, MHWs and SMHWI increased notably heterogeneous in space, with more pronounced increases along the coastline of the ECS (e.g., MHW and SMHWI) and coastline of northern SCS (e.g., HDs). Yao et al. (2020) detected an increasing trend in MHWs, at the rates of 1–2 per decade during 1982–2018, in the China's marginal seas and adjacent offshore waters ( $0^\circ$ – $42^\circ$ N,  $98^\circ$ – $135^\circ$ E). Their results partially agree with these presented in Fig. 2c. Trends in SMHWD have increased across the most China Seas, with some regions exceeding 8 days per decade. Conversely, it is remarkable that cold extremes (CDs, MCSs and severe MCSs), have decreased or weakened over most regions (Fig. 2b, d, 2f, 2h). Trends in cold extremes were also not uniform, with major decreasing tendencies scattered across the western of the Kuroshio Current. There was a small area along the west coast of Korea that displayed modest increase or decrease tendencies for both hot and cold extremes. It was consistent with Lee et al. (2020), who found the SST warming trend is visible only in winter, not in summer.

#### 3.2. Regional averaged temporal variations and trends in ocean temperature extremes

To illustrate the time evolution of SST extremes, the annual metrics were the regional averaged over all grid points of the China Seas ( $15^\circ$ – $45^\circ$ N,  $105^\circ$ – $130^\circ$ E). Yearly time series of these metrics and trends are presented in Fig. 3 and validated in Table 2. Clear trends are observed in the area-averaged ocean temperature metrics. The trends in the frequency of HDs and MHWs have been increased by 9.68 days per decade and 0.96 count per decade, respectively. CDs and MCSs, showed significant decreasing tendency, by rates of 7.5 days per decade and 0.72 count per decade, respectively. Fig. 3e to h shows the SMHWs/SMCSs in each year from 1982 to 2020. We note that the severe MHWs/MCSs are increased/decreased significantly, with a magnitude of  $0.41^\circ$ C ( $-0.24^\circ$ C) per decade and 6.49 ( $-2.80$ ) days per decade, respectively. Hot extremes (HDs, MHWs, SMHWs) have intensified faster than cold extremes (CDs, MCSs, SMCSs) have weakened on a regional scale (Wang et al., 2022). It is worth noting that linear trends of SMHWI and SMHWD are larger than those of annual mean MHW intensity and duration, namely severe MHWs have been become much stronger in the past decades. Both SMHWI and SMHWD play critical roles in fatal heat stress accumulation (McClanahan et al., 2019). More SMHWs could push ecosystems beyond their threshold of recovery; with lasting consequences for marine biodiversity, and millions of people who depend upon them.

The time series show remarkable inter-decadal variations and significant transition points at inter-decadal timescale (Fig. 3). The rapid change in climate indicates the transition of climate from one stable to



**Fig. 2.** Spatial distribution of long-term trends of HDs (a) and CDs (b); MHWs (c) and MCSs (d); SMHWI (e) and SMCSI (f); SMHWD (g) and SMCSD (h) in the China Seas during 1982–2020. Black dots indicate significant trends at 0.05 level using the MK test of each grid point. Note: MCS intensities are by definition negative SSTAs, a positive trend in MCS intensity over time means weakening MCS.

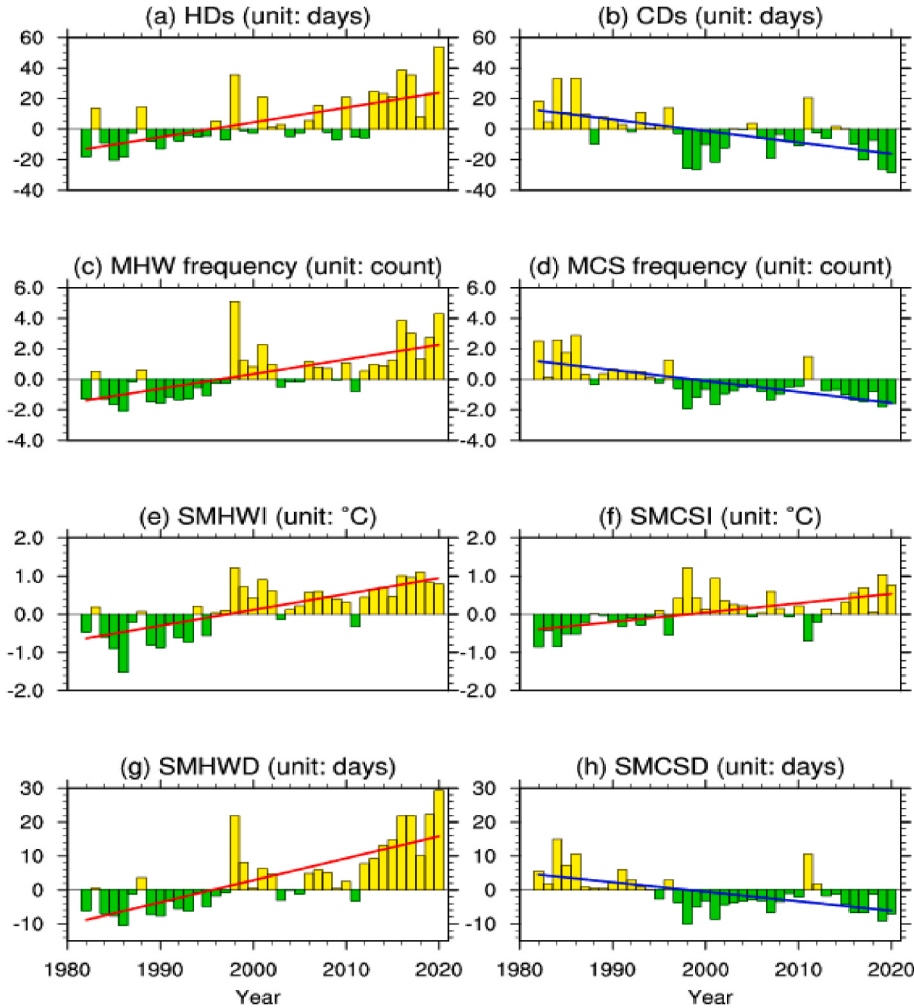


**Fig. 3.** Temporal variations of area-averaged SST extreme indices over the China Seas during 1982–2020; (a) HD; (b) CD; (c) MHW; (d) MCS; (e) SMHWI; (f) SMCSI; (g) SMHWD; (h) SMCSD, relative to 1983–2012 means. Green bar: negative anomaly; yellow bar: positive anomaly; red straight line: positive trend; blue straight line: negative trend. Note that MCS intensities are by definition negative SSTAs, and therefore, a positive trend in MCS intensity over time means weakening MCS. (For interpretation of the references to colour in this figure legend, the reader is referred to the Web version of this article.)

**Table 2**

Trends and their significance of the area-averaged marine temperature extremes from 1982 to 2020. Here,  $p < 0.05$  means that the linear trend was significant at 95% confidence level.  $R^2$  is a statistical measure of how close the data are to the fitted regression line.  $R^2$  is always between 0 and 1, 1 indicates that the model explains all the variability of the response data around its mean.

ID	Type	Trend	Unit	$p$ -value	$R^2$
HDs	/	$9.68 \pm 1.92$	days/decade	1.16e-05	0.41
CDs	/	$-7.50 \pm 1.76$	days/decade	1.27e-04	0.33
MHW	/	$0.96 \pm 0.18$	count/decade	8.06e-06	0.42
MCS	/	$-0.72 \pm 0.13$	count/decade	1.87e-06	0.46
SMHWI	SMHWI	$0.41 \pm 0.06$	°C/decade	1.34e-07	0.53
	SMHWD	$6.49 \pm 0.93$	days/decade	1.47e-04	0.33
SMCS	SMCSI	$0.24 \pm 0.06$	°C/decade	2.95e-08	0.57
	SMCSD	$-2.80 \pm 0.65$	days/decade	1.22e-04	0.33

another (Ullah et al., 2019b). Here, the Mann-Kendall abrupt change test was employed to detect the significance of interdecadal shift in time series. An intersection point of  $UF$  and  $UB$  curves located within the confidence interval indicates the beginning of a step turning point. Overall, through the MK test, all of the turning points were detected around the year 1998 and were significant at the 95% significance level (figure omitted). For the past four decades, the highest frequencies of area-averaged HDs, MHWs and SMHWs occurred in the recent decade (2011–2020) after the turning point year 1998 and the lowest frequencies of HDs, MHWs and SMHWs occurred in the first decade (1982–1991) before the year 1998. The HDs and MHWs increased from

about 29.6 days per year and 1.3 count per year during 1982–1991 to 58.0 days per year and 4 count per year during 2011–2020. Specially, the SMHWI and SMHWD are sharply increased from about 1.2 °C per year and 6.6 days per year during 1982–1991 to 2.41 °C per year and 26.0 days per year during 2011–2020. Cold extremes were relative lower in magnitude but significantly decreased.

### 3.3. Asymmetry between MHWs and MCSs

In section 3.2, we found the asymmetry in the linear trends of MHWs and MCSs. This asymmetry can be explained by the underlying temperature distribution. If the distribution was normally distributed, the warm and cold tails would be symmetric with warm and cold extremes to be of equivalent intensities and opposite in sign. If the distribution is skewed, the intensity of extremes on the skewed side can be expected to be more intense than on the non-skewed side.

Here, to determine how the distribution changed, PDF of area-averaged daily SSTAs were examined. Firstly, we compared the performances of the Gumbel and GEV distributions in the SSTAs, based on cumulative density function (CDF) (Fig. 4a). It noted that both of the GEV and Gumbel model own a tail distribution. However, only the GEV's values fit well at the low and high ends of the observed daily SSTAs. Furthermore, we use quantile-quantile (Q-Q) plot to assess the goodness of fit from the two models (Fig. S1, in Supporting Information S1). The plot from GEV is very close to the 45° line. The comparison also shows that GEV distributions perform better than the Gumbel model. Thus, in Fig. 4b we show the GEV-fit PDFs curves for the two subperiods

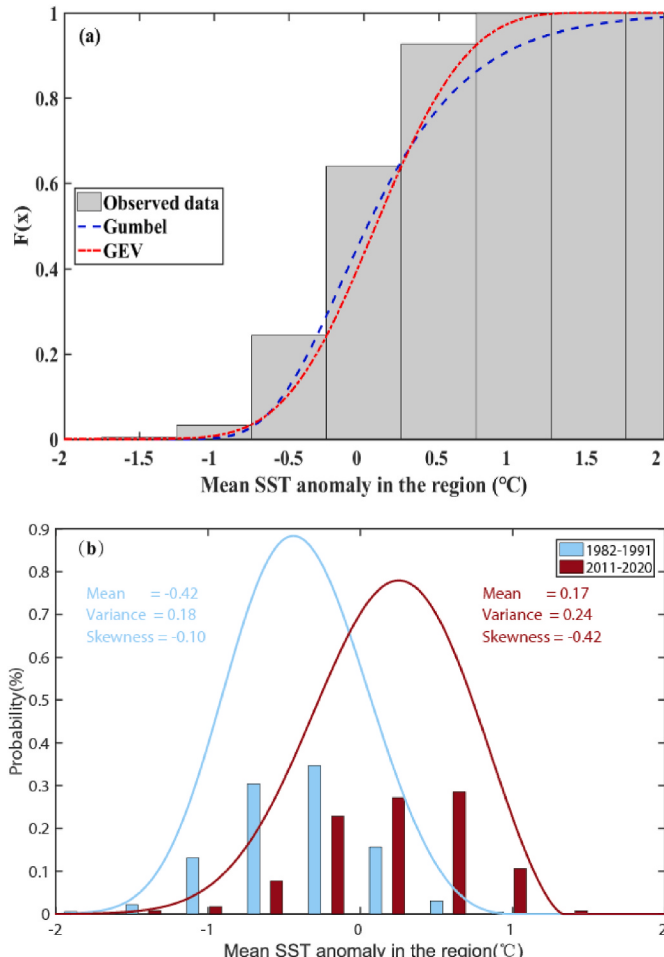


**Fig. 4.** CDF distribution ( $F(x)$ ) of daily SSTAs of the area-averaged during 1982–2020 (a); Histograms and GEV-fit PDFs of the area-averaged daily SSTAs for 1982–1991 (the first decade, blue bars and blue line) and 2011–2020 (the recent decade, red bars and red line) (b). Statistics of the shape, scale, and location parameters are shown in Fig. 4b. (For interpretation of the references to colour in this figure legend, the reader is referred to the Web version of this article.)

in term of the transition point analyzed in 3.2, e.g., 1982–1991; 2011–2020. Meanwhile, the higher moment statistics including, mean, variance, and skewness are also listed.

In all cases the distributions between the two subperiods are shown to be statistically significantly different from each other at the 1% level, generally related with a significant shift in the location parameter (mean) of the PDFs. Both distribution curves of daily SSTAs show a unimodal feature. The mean state has clearly shifted towards higher SSTAs (i.e., from  $-0.42\text{ }^{\circ}\text{C}$  to  $0.17\text{ }^{\circ}\text{C}$ ), implying considerably more frequent and intense high SSTAs, which can increase the likelihood of MHWs or inhibit the likelihood of MCSs. Meanwhile, the curve shape of 2011–2020 was much skewed (with the skewness value of  $-0.42$ ), comparing with the value of  $-0.1$  in 1982–1991. Then the frequency and intensity of hot extremes on the skewed side would be more frequent and intense than cold extremes on the non-skewed side. Therefore, observations analyses imply that the asymmetry of MHWs and MCSs metrics can be explained by the aforesaid temperature distribution.

#### 3.4. SST drivers of MHW/MCS trends

In this section, we focus on MHWs and MCSs. Fig. 5 shows time series of MHW/MCS metrics from  $\text{SST}$ ,  $\text{SST}^{\text{detrend}}$  in the China Seas during 1982–2020 (blue and green bars, respectively). To derive the impact of

the long-term trend of SST ( $\text{SST}^{\text{trend}}$ ) on each MHW/MCS metric (including frequency, SMHWI, SMHWD, red bars in Fig. 5), MHW/MCS metrics calculated from the internal variability component were subtracted from the observed metrics. Results show that MHW metrics derived from  $\text{SST}^{\text{trend}}$  including frequency, SMHWI and SMHWD, all exhibit dramatic upward trends, with the rates of 1.06 event per decade,  $0.40\text{ }^{\circ}\text{C}$  per decade, 5.83 days per decade, respectively. In contrast, there were no secular trends in MHWs derived from  $\text{SST}^{\text{detrend}}$ , with all of the rates do not exceed 95% confidence level. Similarly, the trend in MCS metrics derived from  $\text{SST}^{\text{trend}}$  was significant decreased by 0.7 event per decade,  $0.24\text{ }^{\circ}\text{C}$  per decade, 3.37 days per decade, respectively, but with no secular trends in MCS metrics derived from  $\text{SST}^{\text{detrend}}$ . This could support that both the long-term trends in MHW/MCS metrics since 1982 in the China Seas are driven by the mean warming induced by anthropogenic or natural forcing and not by the variability. We further calculate the TAR of the mean SST and internal variability in long-term trends of MHW/MCS metrics. Result shows that increasing trends of MHW/MCS frequency, SMHWI/SMCSI and SMHWD/SMCSD were primarily driven by mean SST warming, with the TAR values of 1.0/1.0, 1.0/1.0 and 0.87/0.83, respectively.

Noticeably, it also showed that the positive influence (i.e., positive values of red bars) of mean SST increased very rapidly over the last two decades. There are shift around the year 1998 in these metrics time series based on  $\text{SST}^{\text{trend}}$  (Fig. 5, red bars). More MHWs and more severe MHWs from  $\text{SST}^{\text{trend}}$  were seen during the post-1998 era, particularly in the recent decade. When compared to the pre-1998 era, MHWs caused by anthropogenic or natural climate change in the post-1998 era increased very rapidly, while MCSs decreased very rapidly. Specially, in the pre-1998 era, internal variability was the major contributor to the MHW metrics. These time series in the pre-1998 era appear to relate to El Niño-Southern Oscillation (ENSO) events. The peaks align with the 1982/83, 1987/88, 1997/98 El Niño (Fig. 5a, c, e, green bars). SST variability contributed most for the year 1983, with 167%, 126%, and 152% of the MHW metrics from SST time series. Similarly, for MCS metrics time series, the peaks align with the 1984/85, 1995/1996, 2010/2011 La Niña (Fig. 5b, d, f, green bars). Specially, in the after-1998 era, internal variability was the major contributor to the MCS metrics. SST variability contributed most for the year 2010, with 158%, 171%, and 170% of the MCS metrics from SST time series.

## 4. Discussion

The combined analysis of marine hot and cold extremes could reveal information that is not obvious from the investigation of either extreme individually. Our statistical investigation examined the spatial and temporal trends of these marine temperature extremes, as well as how these metrics were expected to be influenced by SST changes during 1982–2020. We found that the tendencies of hot metrics versus cold metrics in the China Seas are asymmetric. Hot metrics showed larger increasing and strengthening trends, whereas cold metrics revealed the lower decreasing and weakening trends. The relationship between changes of MHWs and MCSs remains unclear, though the asymmetry of change rates may be explained by the internal temperature variations.

This is, to our knowledge, the first efforts to quantify the roles of anthropological or natural forcing and internal variability on trends of MHWs/MCSs metrics in the China Seas. Referring to Marin et al. (2020), we took a more practical approach, decomposing the SST time series at each grid pixel into mean SST time series and variability time series. This approach does not evaluate the influence of a change on variance, as done in Oliver (2019), but rather compares the influence of long-term changes in SST with all other modes of variability attributed to internal processes of the Earth's climate system (Marin et al., 2020). The most important finding was that the trends in MHW/MCS metrics in the China Seas were primarily caused by mean SST warming, rather than SST variability.

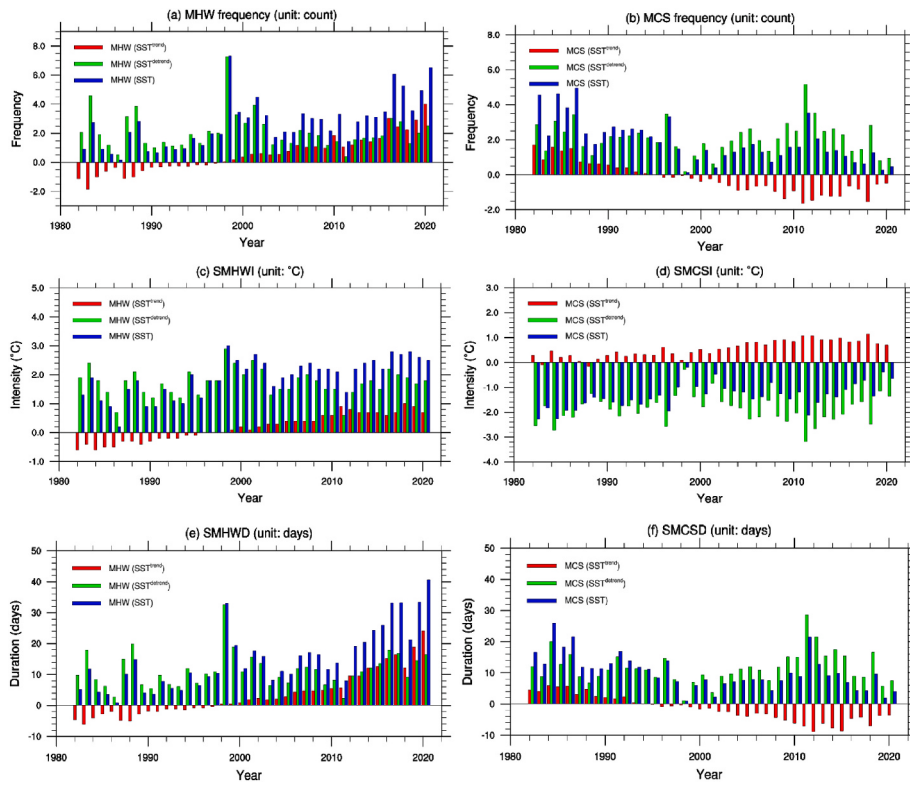


**Fig. 5.** Temporal variations of MHW/MCS frequency (a, b); SMHWI/SMCSI (c, d); SMHWD/SMCSD (e, d) derived from  $SST^{trend}$  (red bars),  $SST^{detrend}$  (green bars), and  $SST$  (blue bars), respectively. Note that MCS intensities are by definition negative SSTAs, therefore, a positive trend in MCS intensity over time means weakening MCS. (For interpretation of the references to colour in this figure legend, the reader is referred to the Web version of this article.)

Hobday et al. (2016) recommended a fixed-baseline period of 30 years for study marine temperature extremes (e.g., 1983–2012, which was also chosen in our work), considering the limited time coverage of SST data and the influence of natural oscillation such as ENSO. However, as the ocean warms, the actual water temperature itself will shift, and rising mean SST might increase MHWs frequency or decrease MCSs frequency. Therefore, some researchers used a full period or recent sub-period, or moving baselines to describe MHWs/MCSs, which is more advantageous for describing the short-term SST fluctuations (Wang et al., 2022; Jacox et al., 2022). To test the sensitivity of the analysis results to baseline choice, we further separately analyzed the data using 1990–2019 (the recent 30-year for climatology) and 1982–2020 (the full period for climatology) baselines (Figs. S2 and S3, in Supporting Information S1). Regardless of the baseline, the asymmetric trends of SMHW/SMCS are robust (Table S1, in Supporting Information S1). However, the results for asymmetric trends of MHW/MCS frequency were found to be sensitive to the baseline choice, with MCS frequency decreasing faster than the increasing trend in MHW frequency using the 1990–2019 baseline, or MCS frequency decreasing rate equal with MHW frequency increasing using the 1982–2020 baseline. The results for SST drivers of MHW/MCS trends were found to be relatively insensitive to baseline choice. This further work confirms that both the long-term trends in MHW/MCS metrics since 1982 in the China Seas are driven by the mean warming brought on by anthropogenic or natural forcing, rather than variability.

Interannual MHWs metrics in the China Seas can also be affected by atmospheric and oceanic modes, including Western North Pacific Sub-tropical High, Baikal High Ridge, ENSO, etc (Li et al., 2019; Tan et al., 2022). Our result confirmed that the peaks in the MHWs metrics align with the 1982/1983, 1987/1988, 1997/1998, 2002/2003 and 2015/2016 El Niño events (Fig. 5a, c, e, green bars). Similarly, for MCS metrics time series, the peaks align with the 1984/85, 1995/1996, 2010/2011 La Niña (Fig. 5b, d, f, green bars). Past studies have

confirmed that, on interannual to intra-seasonal timescales, MCSs have been attributed to several oceanic and atmospheric teleconnection patterns (e.g., ENSO, Arctic Oscillation, North Atlantic Oscillation), through anomalous winds and air-sea heat fluxes, ocean currents and anomalously strong upwelling (Schlegel et al., 2017, 2021; Chiswell 2021).

In long-term timescale, it is expected that in the future continuous SST warming will increase the occurrence of MHWs, particularly the intensification of SMHWs. Meanwhile, according to our study, MCSs are becoming less frequent and SMCSs have been significantly weakening as the atmosphere and oceans warm, indicating that MCS and SMCS will eventually vanish in some areas. For marine ecosystems, this phenomenon might result in a beneficial reduction of cold stress. However, some MCSs are helpful to the marine ecosystem, particularly as ocean temperatures rise and more MHWs are formed, disrupting the ocean's ecological balance. In Australia's west coast, for instance, a sequence of MCSs mitigated the impacts of heat stress and allowed local abalone, scallop and crab fisheries to recover (Schlegel et al., 2021). Thus, fewer MCSs also imply that refuges and recovery periods from MHWs are disappearing, resulting in greater harm.

## 5. Conclusions

The observed changes in marine hot extremes (HDs, MHWs, SMHWs) and cold extremes (CDs, MCSs, SMCSs) in the China Seas from 1982 to 2020 were examined in this study. Furthermore, we investigated how the trends in MHW/MCS metrics were affected by mean SST warming and variability. Following conclusions could be drawn.

- (1) Frequency of HDs and MHWs has significantly increased in the majority of the China Seas; SMHWs have become much stronger and longer. Frequency of CDs and MCSs has significantly decreased; SMCSs have become weaker and shorter. Distributions

- of the trends are all heterogeneous, with the largest magnitudes along the coast.
- (2) Cold extremes decreased, while hot extremes magnitudes increased at a faster rate. The long-term changes of hot and cold extremes were characterized by asymmetry trend.
  - (3) Mean SST warming, not SST variability, was the main driver of the trends in both MHW and MCS metrics. MHWs/MCSs related to the anthropogenic or natural forcing increased very rapidly in the post-1998 era. It is projected that MHWs will continue to increase and become more severe, while MCSs will diminish or even disappear under global warming.

In summary, as the global has warmed, more frequent and intense high temperature extremes have unfolded on land and ocean, with severe consequences (Sun et al., 2014; Arias-Ortiz et al., 2018; Smale et al., 2019). However, research on marine temperature extremes globally and in many regions still lag behind the works on land-based temperature extremes. Our work found that severe MHWs have been much stronger and longer in the China Seas over the past four decades. Long-term mean SST warming induced by anthropogenic GHGs is projected to have a strong effect on MHWs in the future, causing them to become more severe, prolonged, and frequent globally (Frölicher et al., 2018), and seem likely to cause catastrophic harm to mariculture industry (Islam et al., 2020). Thus, for future work, we will emphasize more research into improving the accuracy of the prediction system for MHWs. Regional capacity building for MHW monitoring, prediction and earlier warning systems, in particular, must be strengthened. Scientists need to pay closer attention to these severe MHWs to fully understand their severe and long-lasting impacts on regional marine ecosystems, fisheries and related services. Meanwhile, more work should be conducted on the mariculture species with low thermal safety margin (e.g., sea cucumber *Apostichopus japonicus*) to assess the MHWs' risks in mariculture production and provide suggestions for mitigation and adaptations.

## Author statement

Yan Li: Conceptualization, Data Curation, writing—original draft preparation, Formal analysis, Software; Guoyu Ren: Conceptualization, Methodology, Writing—review and editing; Qingyuan Wang: Methodology, Software, Validation; Lin Mu: Funding acquisition, Supervision.

## Declaration of competing interest

The authors declare that they have no known competing financial interests or personal relationships that could have appeared to influence the work reported in this paper.

## Data availability

Data will be made available on request.

## Acknowledgments

This study was supported by the Natural Science Foundation of China (Grant number 42176017); Shenzhen Science and Technology Program (Grant number KCXFZ20211020164015024); Shenzhen Fundamental Research Program (Grant number JCYJ20200109110220482); and Tianjin Science and Technology Program (Grant number 20JCYBJC00640).

## Appendix A. Supplementary data

Supplementary data to this article can be found online at <https://doi.org/10.1016/j.wace.2023.100553>.

## References

- Arias-Ortiz, A., et al., 2018. A marine heatwave drives massive losses from the world's largest seagrass carbon stocks. *Nat. Clim. Change* 8, 338–344.
- Banzon, V., Smith, T.M., Chin, T.M., Liu, C., Hankins, W., 2016. A long-term record of blended satellite and in situ sea-surface temperature for climate monitoring, modeling and environmental studies. *Earth Syst. Sci. Data* 8, 165–176.
- Banzon, V., Smith, T.M., Steele, M., Huang, B., Zhang, H.M., 2020. Improved estimation of proxy sea surface temperature in the Arctic. *J. Atmos. Ocean. Technol.* 37, 341–349.
- Benthuyzen, J.A., Oliver, E.C.J., Feng, M., Marshall, A.G., 2018. Extreme marine warming across tropical Australia during austral summer 2015–2016. *J. Geophys. Res.: Oceans* 123, 1301–1326.
- Chatterjee, A., Anil, G., Shenoy, L., 2022. Marine heatwaves in the Arabian sea. *Ocean Sci.* 18, 639–657.
- Chiswell, S.M., 2021. Atmospheric wavenumber-4 driven South Pacific marine heat waves and marine cool spells. *Nat. Commun.* 12, 1–8.
- Darmaraki, S., et al., 2019. Future evolution of marine heatwaves in the Mediterranean Sea. *Clim. Dynam.* 53, 1371–1392.
- Frölicher, T.L., Fischer, E.M., Gruber, N., 2018. Marine heatwaves under global warming. *Nature* 560 (7718), 360–364.
- Goubanova, K., Li, L., 2007. Extremes in temperature and precipitation around the Mediterranean basin in an ensemble of future climate scenario simulations. *Global Planet. Change* 57, 27–42.
- Hobday, A.J., et al., 2016. A hierarchical approach to defining marine heatwaves. *Prog. Oceanogr.* 141, 227–238.
- Hobday, A.J., et al., 2018. Categorizing and naming marine heatwaves. *Oceanogr.* 31, 162–173.
- Huang, W.K., Stein, M.L., McInerney, D.J., Sun, S., Moyer, E.J., 2016. Estimating changes in temperature extremes from millennial-scale climate simulations using generalized extreme value (GEV) distributions. *Adv. Stat. Clim. Meteorol. Oceanogr.* 2, 79–103.
- Hughes, T.P., Kerry, J.T., Alvarez-Noriega, M., Alvarez-Romero, J.G., Anderson, K.D., Baird, A.H., et al., 2017. Global warming and recurrent mass bleaching of corals. *Nature* 543, 373–377.
- Islam, M.J., Slater, M.J., Kunzmann, A., 2020. What metabolic, osmotic and molecular stress responses tell us about extreme ambient heatwave impacts in fish at low salinities: the case of European seabass. *Dicentrarchus labrax*. *Sci. Total Environ.* 749, 141458.
- Jacox, M.G., Alexander, M.A., Amaya, D., et al., 2022. Global seasonal forecasts of marine heatwaves. *Nature* 604, 486–490.
- Laufkötter, C., Zscheischler, J., Frölicher, T.L., 2020. High-impact marine heatwaves attributable to human-induced global warming. *Science* 369, 1621–1625.
- Lee, S., Park, M.S., Kwon, M., Kim, Y.H., Park, Y.G., 2020. Two major modes of east Asian marine heatwaves. *Environ. Res. Lett.* 15, 074008.
- Li, Y., Ren, G.Y., Wang, Q.Y., Mu, L., Niu, Q., 2022. Marine heatwaves in the South China Sea: tempo-spatial pattern and its association with large-scale circulation. *Remote Sens.* 14, 5829.
- Li, Y., Ren, G.Y., Wang, Q.Y., You, Q.L., 2019. More extreme marine heatwaves in the China Seas during the global warming hiatus. *Environ. Res. Lett.* 14, 104010.
- Lima, F.P., Wethay, D.S., 2012. Three decades of high-resolution coastal sea surface temperature reveal more than warming. *Nat. Commun.* 3, 704.
- Marin, M., Feng, M., Philips, H., Bindoff, N., 2020. A global, multiproduct analysis of coastal marine heatwaves: distribution, characteristics, and long-term trends. *J. Geophys. Res.: Oceans* 126, e2020JC016708.
- Matich, P., Strickland, B.A., Heithaus, M.R., 2020. Long-term monitoring provides insight into estuarine top predator (*Carcharhinus leucas*) resilience following an extreme weather event. *Mar. Ecol. Prog. Ser.* 639, 169–183.
- McClanahan, T.R., Darling, E.S., Maina, J.M., Muthiga, N.A., Stéphanie, D'agata, Jupiter, S.D., et al., 2019. Temperature patterns and mechanisms influencing coral bleaching during the 2016 El Niño. *Nat. Clim. Change* 9, 845–851.
- Oliver, E.C.J., 2019. Mean warming not variability drives marine heatwave trends. *Clim. Dynam.* 53, 1653–1659.
- Oliver, E.C.J., Benthuyzen, J.A., Sofia, Darmaraki, Donat, M.G., Hobday, A.J., Holbrook, N.J., Schlegel, R.W., Gupta, A.S., 2021. Marine heatwaves. *Ann. Rev. Mar. Sci.* 13, 313–342.
- Sen, P.K., 1968. Estimates of regression coefficient based on Kendall's tau. *J. Am. Stat. Assoc.* 63, 1379–1389.
- Schlegel, R.W., Oliver, E.C.J., Sarah, P.K., Andries, K., Smit, A.J., 2017. Predominant Atmospheric and oceanic patterns during coastal marine heatwaves. *Front. Mar. Sci.* 4, 323.
- Schlegel, R.W., Darmaraki, S., Benthuyzen, J.A., Filbee-Dexter, K., Oliver, E.C.J., 2021. Marine cold-spells. *Prog. Oceanogr.* 198, 102684.
- Smale, D.A., Wernberg, T., Oliver, E.C.J., Thomsen, M., Harvey, B.P., Straub, S.C., et al., 2019. Marine heatwaves threaten global biodiversity and the provision of ecosystem services. *Nat. Clim. Change* 9, 306–312.
- Sun, Y., et al., 2014. Rapid increase in the risk of extreme summer heat in Eastern China. *Nat. Clim. Change* 4, 1082–1085.
- Tabari, H., Abghari, H., Talaei, P.H., 2012. Temporal trends and spatial characteristics of drought and rainfall in arid and semiarid regions of Iran. *Hydrol. Process.* 26, 3351–3361.
- Tan, H.J., Cai, R.S., Wu, R.G., 2022. Summer marine heatwaves in the South China Sea: trend, variability and possible causes. *Adv. Clim. Change Res.* 13, 323–332.
- Ullah, S., You, Q., Ullah, W., Ali, A., Xie, W., Xie, X., 2019a. Observed changes in temperature extremes over China-Pakistan Economic Corridor during 1980–2016. *Int. J. Climatol.* 39 (3), 1457–1475.

- Ullah, S., You, Q., Ullah, W., Ali, A., 2019b. Observed changes in maximum and minimum temperatures over China-Pakistan economic corridor during 1980-2016. *Atmos. Res.* 216, 37–51.
- Wang, D., Xu, T., Fang, G., Jiang, S., Wang, G., Wei, Z., Wang, Y., 2022. Characteristics of marine heatwaves in the Japan/east sea. *Rem. Sens.* 14, 936.
- Wang, Y., Kajtar, J., Alexander, L.V., Pilo, G.S., Holbrook, N.J., 2022. Understanding the changing nature of marine cold-spells. *Geophys. Res. Lett.* 49, e2021GL097002.
- Yao, Y., Wang, J., Yin, J., Zou, X., 2020. Marine heatwaves in China's marginal seas and adjacent offshore waters: past, Present, and Future. *J. Geophy. Res.: Oceans* 125, e2019JC015801.
- Zhang, P., Ren, G., Xu, Y., Qin, Y., Sun, Y., Wang, X., 2019. Observed change in extreme temperature over the global land based on the newly developed CMA daily dataset. *J. Clim.* 32, 8489–8509.
- Zwiers, F., Zhang, X., Feng, Y., 2011. Anthropogenic influence on long return period daily temperature extremes at regional scales. *J. Clim.* 24, 881–892.